INTERNATIONAL JOURNAL OF HYDROGEN ENERGY 37 (2012) 6199–6214

Available at www.sciencedirect.com

ScienceDirect

journal homepage: www.elsevier.com/locate/he

Inorganic–organic membranes based on Nafion, $[(ZrO_2)\cdot(HfO_2)_{0.25}]$ and $[(SiO_2)\cdot(HfO_2)_{0.28}]$. Part I: Synthesis, thermal stability and performance in a single PEMFC

Vito Di Noto [a,b,*,1], Nicola Boaretto [a], Enrico Negro [a], Guinevere A. Giffin [a], Sandra Lavina [a], Stefano Polizzi [c]

[a] Dipartimento di Scienze Chimiche, Università di Padova, Via Marzolo 1, I-35131 Padova (PD), Italy
[b] Istituto di Scienze e Tecnologie Molecolari, ISTM-CNR and INSTM, Dipartimento di Scienze Chimiche, Via Marzolo 1, I-35131 Padova (PD), Italy
[c] Dipartimento di Chimica Fisica, Universit'a di Venezia, Via Torino 155, I-30170 Mestre (Ve), Italy

ARTICLE INFO

Article history:
Received 4 March 2011
Received in revised form
26 July 2011
Accepted 29 July 2011
Available online 9 September 2011

Keywords:
Hybrid inorganic–organic proton-conducting membranes
Nafion
Polymer electrolyte membrane fuel cells
Water uptake
Thermogravimetric measurements
Fabrication and testing of membrane-electrode assemblies

ABSTRACT

This work reports the preparation, characterization and test in a single fuel cell of two families of hybrid inorganic-organic proton-conducting membranes, each based on Nafion and a different "core-shell" nanofiller. Nanofillers, based on either a ZrO_2 "core" covered with a HfO_2 "shell" (ZrHf) or a HfO_2 "core" solvated by a "shell" of SiO_2 nanoparticles (SiHf), are considered. The two families of membranes are labelled [Nafion/$(ZrHf)_x$] and [Nafion/$(SiHf)_x$], respectively. The morphology of the nanofillers is investigated with high-resolution transmission electron microscopy (HR-TEM), energy dispersive X-ray spectroscopy (EDX) and electron diffraction (ED) measurements. The mass fractions of nanofiller *x* used for both families are 0.05, 0.10 or 0.15. The proton exchange capacity (PEC) and the water uptake (WU) of the hybrid membranes are determined. The thermal stability is investigated by high-resolution thermogravimetric measurements (TGA). Each membrane is used in the fabrication of a membrane-electrode assembly (MEA) that is tested in single-cell configuration under operating conditions. The polarization curves are determined by varying the activity of the water vapour (a_{H2O}) and the back pressure of the reagent streams. A coherent model is proposed to correlate the water uptake and proton conduction of the hybrid membranes with the microscopic interactions between the Nafion host polymer and the particles of the different "core–shell" nanofillers.

1. Introduction

Fuel cells (FCs) are advanced electrochemical devices for energy conversion that obtain electric power from the chemical energy of their reagents with a very high yield, up to 55% or more [1]. One family of FCs that has drawn considerable attention from both the academic world and industry is based on two porous electrodes coated with suitable electrocatalysts, where the reactions involved in the operation of the device occur and separated by a proton-exchange membrane (PEM) [2–4]. Systems based on PEMs are known as proton-exchange membrane fuel cells (PEMFCs) and have been

* *Corresponding author*. Dipartimento di Scienze Chimiche, Università di Padova, Via Marzolo 1, I-35131 Padova (PD), Italy. Tel./fax: +39 (0) 498275229.
E-mail address: vito.dinoto@unipd.it (V. Di Noto).
[1] Active ACS, ECS and ISE member.
0360-3199/$ – see front matter
doi:10.1016/j.ijhydene.2011.07.132

extensively studied as power sources for a variety of applications from portable electronic devices to light-duty vehicles owing to their low operation temperature ($T < 130$ °C), high conversion efficiency and high power density in comparison to competing technologies such as lithium batteries and conventional thermal engines [1,4,5]. PEMs can be manufactured from a number of materials, including sulfonated polyetherether sulfones, polyetherethereketones, polysiloxanes, and others [6–8]. However, perfluorinated ionomers, such as Nafion®, Aquivion, Aciplex, among others, are still the most widely applied systems owing to their high proton conductivity and good chemical and electrochemical stability[2] [9–11]. Nevertheless, perfluorinated ionomers suffer from important drawbacks, including the necessity of a very high degree of hydration for proton conduction. This fact ultimately prevents them from operating effectively at temperatures higher than ca. 80–90 °C and low humidification [7,9,12]. These are important technological limitations as: (a) the required water and thermal management modules are very bulky and expensive; and (b) it is necessary to use very pure fuels because at temperatures lower than 120–140 °C the platinum-based electrocatalysts used in PEMFCs show a very poor tolerance towards even small traces of common contaminants such as CO and H_2S [13] that typically are found in hydrogen obtained from steam-reforming processes [14,15]. One way to address the limitations of perfluorinated ionomers is to devise hybrid inorganic–organic proton-conducting materials, where a suitable filler of micrometer to nanometer size is added to the polymer host [16–18]. In recent years, this approach has been focused on a variety of hybrid systems, which utilize the following families of nanofillers [18–33]: (a) heteropolyacids, including silicotungstic acid, phosphotungstic acid, molybdophosphoric acid and others; (b) zirconium phosphate; (c) organically-modified silicates and silane-based fillers; (d) zeolites; and (e) Pt, Pt–SiO_2 and Pt–TiO_2. Generally, the filler is a material characterized by a strongly acidic and/or hydrophilic behaviour. This choice is based on the assumption that these properties would possibly provide extra mobile protons as charge carriers and help the resulting hybrid system retain water at high temperatures and low hydration levels. In the past few years, this research group has conducted experiments on a number of different hybrid systems, to obtain doped Nafion ionomers containing: (a) both pristine and "core–shell" oxoclusters [34–40]; (b) single inorganic oxoclusters doped with an ionic liquid [41]; (c) oxoclusters functionalized with perfluoroalkylated chains [42]; and (d) proton-conducting ionic liquids (PCILs) [43]. These continuing efforts allow better elucidation of the effects arising from the complex interplay between the perfluorinated ionomer and the dopants in terms of structure and the proton conduction mechanism of hybrid proton-conducting materials. Among the investigated materials, systems including nanofillers with a basic character such as HfO_2 have shown an improved proton conductivity and interesting structural features [35–37]. However, the use of pristine hafnium oxide as a filler in hybrid membranes should be avoided because of its very high cost. Recently, it was shown that it is possible to develop oxide nanofillers characterized by "core–shell" morphology. The "core" is made of particles with a high Mohs hardness or crystallinity, while the "shell" consists of the softer oxide [38,39]. This approach is followed here to prepare nanofillers characterized by a HfO_2 "shell" or "core". The ultimate goal is to reduce the loading of hafnium in the resulting hybrid inorganic–organic membranes. ZrO_2 and SiO_2 are used as the "core" and the "shell" to obtain nanofillers with the formulae $[(ZrO_2)\cdot(HfO_2)_{0.25}]$ and $[(SiO_2)\cdot(HfO_2)_{0.28}]$, respectively, which are characterized by HR-TEM, EDX and ED measurements. Two families of hybrid Nafion-based inorganic–organic proton-conducting membranes are prepared with $[(ZrO_2)\cdot(HfO_2)_{0.25}]$ and $[(SiO_2)\cdot(HfO_2)_{0.28}]$ nanofillers and are labelled [Nafion/$(ZrHf)_x$] and [Nafion/$(SiHf)_x$], respectively. In both families, the mass fraction of the nanofiller x is 0.05, 0.10 or 0.15. This study is focused on elucidating the effect of the nanofillers on the proton exchange capacity, water uptake, thermal stability and fuel cell performance of the Nafion host polymer. Particular attention is dedicated to creating a coherent picture that relates the effects of the different Nafion-nanofiller interactions to the water uptake and proton conductivity of the hybrid membranes as a function of the water vapour activity (a_{H2O}) in the environment.

2. Experimental

2.1. Reagents

A 5 wt% solution of Nafion® ionomer with a proton exchange capacity (PEC) of 0.9 mequiv g^{-1} (Alfa Aesar, ACS) was used as received. Amorphous silica with a particle size of 9 μm and a porosity of 1.8 mL g^{-1} was provided by Silysiamont S.p.A., Italy. Zirconium oxide, hafnium oxide and all the solvents were acquired from Sigma–Aldrich and used as received. Nafion 115™ membranes were obtained from Sigma–Aldrich and activated by the standard procedure reported elsewhere [42]. The C2-20 electrocatalyst, used in the preparation of all MEAs, had a platinum loading equal to 20 wt% and was used as received from BASF. Double-distilled water was used in all procedures.

2.2. Preparation of the "core–shell" nanofillers

The $[(ZrO_2)\cdot(HfO_2)_{0.25}]$ nanofiller (ZrHf) was prepared according to the following procedure. 10 mL of a dimethylformamide (DMF) suspension containing 1.5 g of ZrO_2 and 0.643 g of HfO_2 was ground for 10 h at 500 rpm in a tungsten carbide jar using a planetary ball mill. The viscous suspension was transferred into a 100 mL volumetric flask and diluted with DMF. $[(SiO_2)\cdot(HfO_2)_{0.28}]$ nanofiller (SiHf) was obtained according to the same procedure, but the ZrO_2 was replaced with 1.5 g of amorphous silica.

2.3. Membrane preparation

The hybrid inorganic–organic membranes, labelled [Nafion/$(ZrHf)_x$] and [Nafion/$(SiHf)_x$], were prepared by a standard solvent-casting procedure [39]. The nanofiller mass fraction x

[2] The DuPont Oval Logo, DuPont™, the miracles of science™ and all products denoted with a™ and ® are trademarks or registered trademarks of DuPont or its affiliates.

was equal to 0.05, 0.10 or 0.15. Membranes prepared without filler, labelled "pristine recast Nafion", were used as a reference for the PEC, WU and HR-TG measurements. A suitable amount of Nafion, suspended in DMF and prepared as described elsewhere [34,35], was added to a suitable amount of the suspension of nanofiller to obtain a total dry mass of 0.45 g. The mixture was homogenized by sonication and cast onto a Petri dish with a diameter of 5 cm at 100 °C for 15 h. The resulting membranes (thickness of ca. 110 μm) were further treated and purified as described in a previous work [42]. All the membranes were dried for one night at room temperature under a dry air flow before the HR-TG analyses and fabrication of MEAs.

2.4. *Fabrication of membrane-electrode assemblies (MEAs)*

MEAs were prepared with a catalyst-coated substrate (CCS) procedure as described elsewhere [44]. The platinum loading on both the anodic and the cathodic electrocatalyst layers was 0.4 mg cm^{-1}. The Nafion/C ratio was 0.6 [45]. The electrocatalytic layers were deposited on GDS1120 carbon paper obtained from Ballard Power Systems. The resulting gas-diffusion electrodes (GDEs) were hot-pressed onto the membranes according to a protocol detailed elsewhere [46].

2.5. *Instruments and methods*

The proton exchange capacity (PEC) of the membranes was determined as follows [34,35]. 100 mg of each sample were suspended in 100 mL of a 1 M KCl solution. The suspension was stirred overnight and titrated with a 10^{-3} M KOH solution using phenolphthalein as the indicator. The isopiestic water adsorption at different relative humidity values was determined by equilibrating each sample with different saturated salt solutions for two weeks [47]. After recording their weight, the hydrated samples were dried over P_2O_5 for two more weeks and weighted again. The water uptake was converted into the hydration number λ (number of water molecules per sulfonic acid group) by the following formula:

$$\lambda = \frac{wt_{hy} - wt_{dry}}{wt_{dry}} \times \frac{EW}{MW_{H_2O} \cdot (1 - x)} \quad (1)$$

where wt_{hy} is the weight of the hydrated sample, wt_{dry} is the weight of the dry sample, MW_{H2O} is the molecular weight of water, EW is the equivalent weight of Nafion and x is the mass fraction of nanofiller in the hybrid membrane. High-resolution thermogravimetric analyses were carried out with a High Resolution TGA 2950 (TA Instruments) thermobalance. A working N_2 flux of 100 mL min^{-1} was used. The TG profiles were collected in the temperature range between 20 and 900 °C, using an open platinum pan loaded with ca. 7 mg of each material.

High resolution transmission electron microscopy (HR-TEM) and electron diffraction (ED) were performed using a Jeol 3010 instrument operated at 300 kV with a high-resolution pole piece (0.17 nm point-to-point resolution) and equipped with a Gatan slow-scan 794 CCD camera. Energy-dispersive X-ray spectroscopy (EDX) was carried out using an Oxford Instrument EDS detector (Mod. 6636). The sample powders were suspended in isopropanol and a 5 μL drop of this suspension was deposited on a porous carbon film supported on 3 mm copper grid.

2.6. *Tests in a single-cell configuration*

Single fuel cell tests were carried out in a 5 cm^2 single cell with a two-channel serpentine flow field for both the anodic and the cathodic sides, using pure hydrogen as the fuel and pure oxygen or air as the oxidant. The temperature of the cell and reagent streams was kept constant at 85 °C. The hydrogen flow rate was 800 ml·min^{-1}. Air and oxygen flow rates were set at 1700 and 500 ml·min^{-1}, respectively. Polarization curves were collected with fully-humidified reagent streams at a back pressure of 4 bar and then at a back pressure of 1 bar. Subsequently, the activity of the water vapour (a_{H2O}) of both reagent streams was reduced to 0.75 and the polarization curves were measured after the system reached stability. Finally, polarization curves were determined with both reagent streams having the same a_{H2O} of 0.50, 0.25, 0.12 or 0.05. All the measurements with reagent streams characterized by $a_{H2O} < 1$ were collected at a back pressure of 1 bar. Both pure oxygen and air were used as oxidants at each set of operating conditions. The polarization curves were not corrected for internal resistance losses.

3. Results

3.1. *Preparation of the nanofillers*

To obtain the nanofillers described here, two oxides characterized by a different Mohs hardness or crystallinity are suspended in dimethylformamide (DMF). The resulting mixture is ground extensively in a planetary ball mill. There are two main objectives of this preparation protocol: (a) to segregate the oxide characterized by the lower hardness or crystallinity, i.e. HfO_2 or SiO_2, on the surface of the resulting "core–shell" inorganic biphasic nanoparticles; and (b) to obtain nanoparticles with a very fine and homogeneous granulometry. Both of these objectives were reached for similar "core–shell" systems prepared by the same procedure [38,39]. "Core-shell" inorganic nanodomains can be divided into two classes: chemical and physical "core–shell" nanodomains. In chemical "core–shell" nanodomains, a "core" with a higher Mohs hardness index or with a higher crystallinity is chemically covered by a "shell" of a softer material characterized by a lower Mohs hardness. A chemical bonding interaction occurs between the shell and the core materials when the two materials have compatible crystal structures and chemical behaviour ("core–shell" type A). In the physical "core–shell" nanodomains, a simple adhesion of the soft phase, characterized by a low Mohs hardness or less crystalline nanoparticles, onto the surface of the nanoparticles with a high Mohs hardness is expected. Physical "core–shell" nanoparticles occur when the two materials forming the "core–-shell" have very different and incompatible crystal structures. In this situation, the soft phase is physically adsorbed on the surface of the hard nanoparticles to form a physically-interacting shell ("Core–Shell" type B).

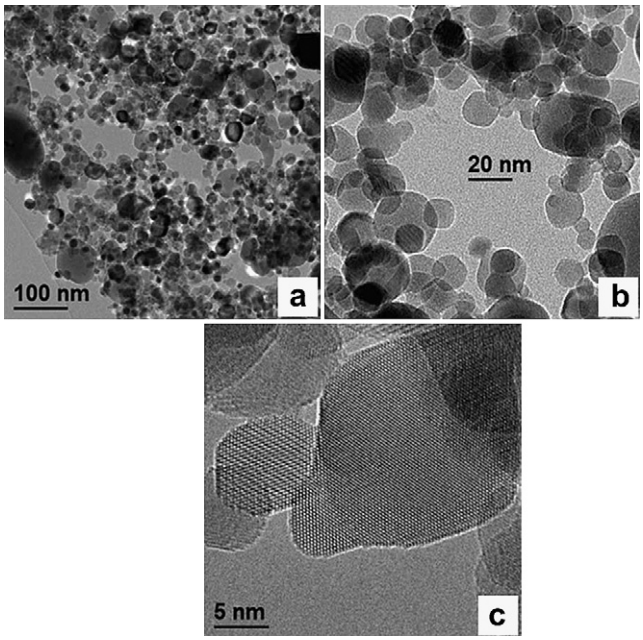

Fig. 1 – HR-TEM morphology images of ZrHf "core–shell" nanofiller.

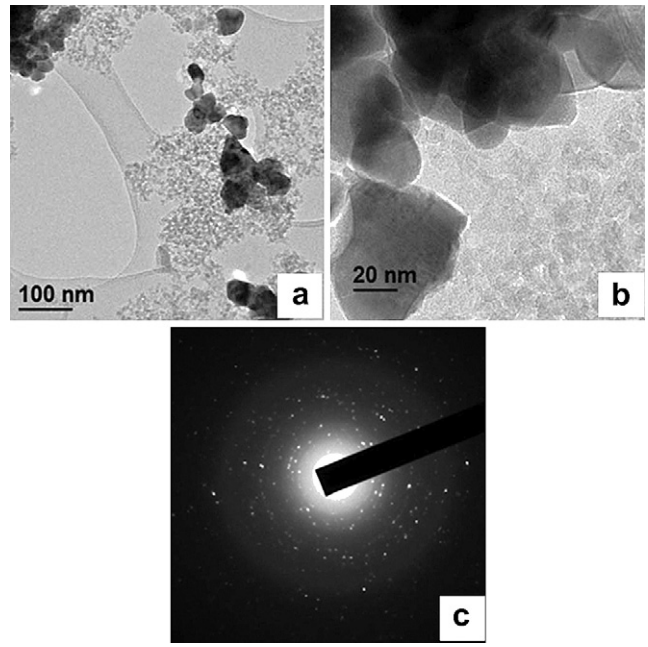

Fig. 2 – HR-TEM morphology images (a) and (b) and electron diffraction pattern (c) of SiHf "core–shell" nanofiller.

The ZrHf and SiHf fillers were carefully characterized by HR-TEM. The micrograph in Fig. 1(a) indicates that ZrHf consists of nanoparticles with an approximately spherical shape and diameters ranging from 10 to 100 nm. The particles sizes are classified on the basis of EDX analyses: a) large nanoparticles ($d > 80$ nm) with atomic percentages of Zr = 49.6, Hf = 0.6 and O = 49.8% at; b) medium nanoparticles ($20 \leq d \leq 80$ nm) with Zr = 44.2, Hf = 1.3 and O = 54.3% at; and c) small nanoparticles ($d < 20$ nm) with Zr = 40.8, Hf = 5.9 and O = 53.3% at. It should be observed that decreasing the particle size increases the ratio of the atomic percentages Hf/Zr, which indicates that the thickness of the layer of the soft material interacting with the surface of hard core is probably independent of the "core" size. Fig. 1(b) and (c) show the morphology of the smaller particles. It is impossible to distinguish the ZrO_2 and HfO_2 phases by electron diffraction measurements and HR-TEM. The results demonstrate that these two components are isomorphous phases and as shown in Fig. 1(c) the particles are highly crystalline with interplanar distances corresponding to a polyphasic α-ZrO_2, composed of triclinic α-ZrO_2 (P_{4_2}/nmc) with small amounts of monoclinic ($Fm\overline{3}m$) and cubic (P_{21}/c) α-ZrO_2. The interplanar distances also correspond to a triclinic HfO_2 (P_{4_2}/nmc). From these results, it should be concluded that the HfO_2 soft phase is highly compatible with the ZrO_2 nanoparticles. It is chemically bonded to the surface of the ZrO_2 "core" nanoparticle forming a "shell" with an isomorphic structure making ZrHf a good example of an A-type "core–shell" nanofiller.

The micrographs in Fig. 2(a) and (b) clearly show that the SiHf filler consists of crystalline HfO_2 nanoparticles with diameters ranging from 50 to 100 nm and a "shell" of tiny amorphous grains of SiO_2 with sizes lower than 10 nm physically adsorbed on the surface of the HfO_2 nanoparticles. These results were supported by the EDX analyses and the electron diffraction measurements shown in Fig. 2(c). EDX measurements revealed a clear phase segregation between the "core" and the "shell" domains of the nanoparticles. The electron diffraction pattern of Fig. 2(c) exhibits the typical structure of amorphous silica grains revealed as a diffuse "halo" and shows that HfO_2 is present in its original crystalline structure. From this information, it is concluded that SiO_2 and HfO_2 are completely chemically incompatible and the "core–shell" morphology of HfO_2 and SiO_2 results from a physical adhesion of SiO_2 on the surface of HfO_2. Thus, the SiHf is a B-type "core–shell" nanofiller.

3.2. *Preparation of the hybrid membranes*

To incorporate particles characterized by a very fine granulometry, it is essential to expand their contact area with the polymer host matrix to promote the effects arising from the interactions between the two components in the resulting hybrid inorganic–organic material. The suspension of the nanofillers and the Nafion ionomer in DMF is particularly stable. This is very important to inhibit the settlement of the nanofiller particles during the solvent-casting procedure. The hybrid membranes are homogeneous and characterized by a uniform thickness of ca. 110 μm. This value was chosen to approximately match the thickness of the Nafion 115 reference membrane. The MEAs assembled from these hybrid systems are expected to show good performances and minimize the issues arising from the crossover of the reagents or the development of pinholes and cracks in the membrane. The treatments performed after the solvent-casting procedure, i.e. the consolidation of the [Nafion/$(ZrHf)_x$] and [Nafion/

Table 1 – Proton exchange capacity of [Nafion/(ZrHf)$_x$] and [Nafion/(SiHf)$_x$] hybrid membranes.

x	PEC (mequiv g^{-1})		
	Nominal[a]	[Nafion/(ZrHf)$_x$][b]	[Nafion/(SiHf)$_x$][b]
0	0.9	0.9	0.9
0.05	0.855	0.86	0.87
0.1	0.810	0.8	0.82
0.15	0.765	0.78	0.8

a Calculated by correcting the PEC of Nafion by the mass fraction of nanofiller.
b Determined by titration.

(SiHf)$_x$] hybrid membranes at 130 °C for 3 h followed by a hot-pressing step at 100 °C and 1000 psi, are intended to: (a) remove the last traces of solvents; (b) consolidate the mechanical properties of the hybrid materials; and (c) prevent the irreversible swelling of the membranes in the subsequent washing procedures.

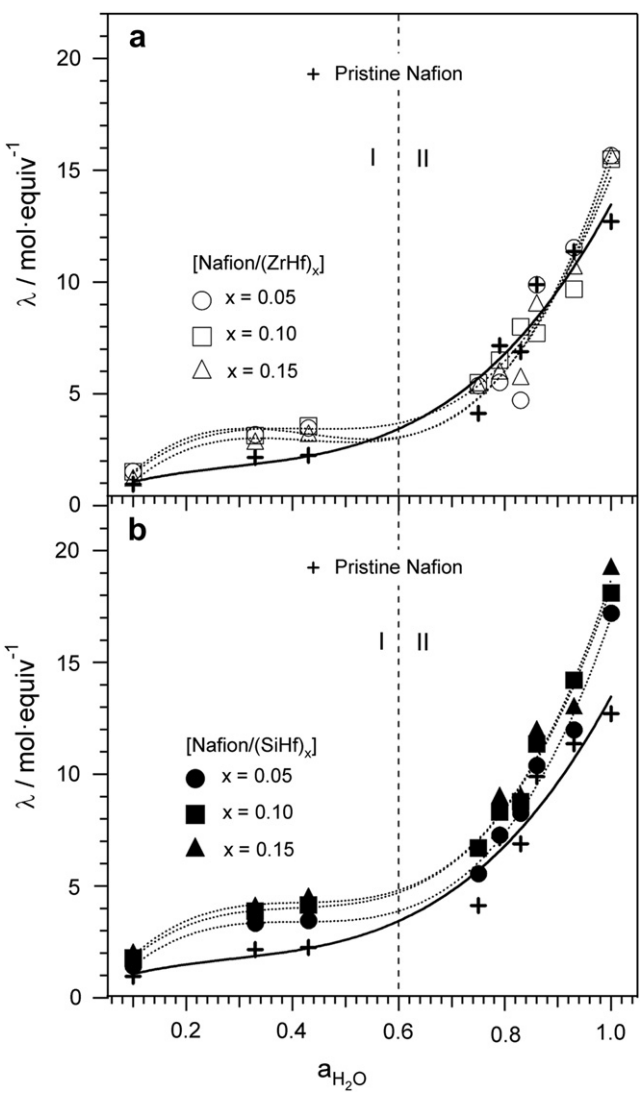

Fig. 3 – Dependence of λ versus the water activity (a_{H2O}) for the hybrid membranes; values determined by isopiestic absorption. (a) [Nafion/(ZrHf)$_x$] membranes; (b) [Nafion/(SiHf)$_x$] membranes. The lines are meant as a guide for the eye.

3.3. *Proton exchange capacity (PEC) and water uptake*

The proton exchange capacity (PEC) values of both the [Nafion/(ZrHf)$_x$] and the [Nafion/(SiHf)$_x$] membranes are determined by titration as discussed in Section 2.5 and are shown in Table 1. Both families of membranes are characterized by PEC values very similar to the nominal figures obtained by correcting the PEC of pristine Nafion according to its mass fraction in the hybrid systems. Therefore, the nanofillers do not provide any significant additional contribution to the PEC of either the [Nafion/(ZrHf)$_x$] or [Nafion/(SiHf)$_x$] membranes. The values of λ determined by the isopiestic absorption of water at various water activities are shown in Fig. 3 [47]. It is possible to divide the graphs into two regions, I and II. I includes the data collected at water activities below 0.6, while II covers the remaining data. In I, the evolution of λ is moderate and follows a Langmuir-like trend. Both [Nafion/(ZrHf)$_x$] and [Nafion/(SiHf)$_x$] membranes show a higher λ than pristine recast Nafion in region I. Fig. 4 reports the values of λ versus the mass fraction of nanofiller x for both families of hybrid membranes at $a_{H2O} = 0.33$ and $a_{H2O} = 1$. It is observed at $a_{H2O} = 0.33$ (upper panel of Fig. 4) that: (a) the λ values for [Nafion/(SiHf)$_x$] membranes are larger than those of the [Nafion/(ZrHf)$_x$] membranes for all x; and (b) λ increases as x increases in [Nafion/(SiHf)$_x$] membranes. In comparison, the maximum λ occurs at $x = 0.05$ for [Nafion/(ZrHf)$_x$] membranes before undergoing a very slight decrease as x increases to 0.15. Similar trends are observed at $a_{H2O} = 1$ (lower panel of Fig. 4), except there is no significant decrease in λ as observed in [Nafion/(ZrHf)$_x$] membranes at $x = 0.1$ and $x = 0.15$. It should be highlighted that in region II, $a_{H2O} > 0.7$, the differences in λ between the various membranes are increasingly evident, especially for [Nafion/(SiHf)$_x$] membranes. In summary, the introduction of the B-type "core–shell" nanofiller [$(SiO_2)\cdot(HfO_2)_{0.28}$] leads to a significant increase in the capability of [Nafion/(SiHf)$_x$] membranes to absorb water as

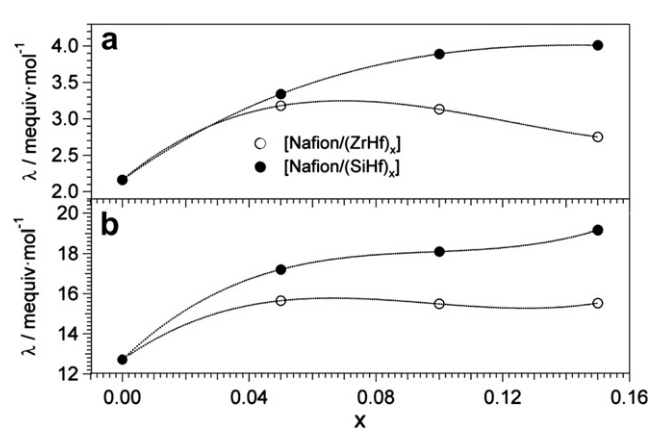

Fig. 4 – Dependence of λ vs. the mass fraction of nanofiller x for the hybrid membranes; values determined by isopiestic absorption at: (a) $a_{H2O} = 0.33$; (b) $a_{H2O} = 1$. The lines are meant as a guide for the eye.

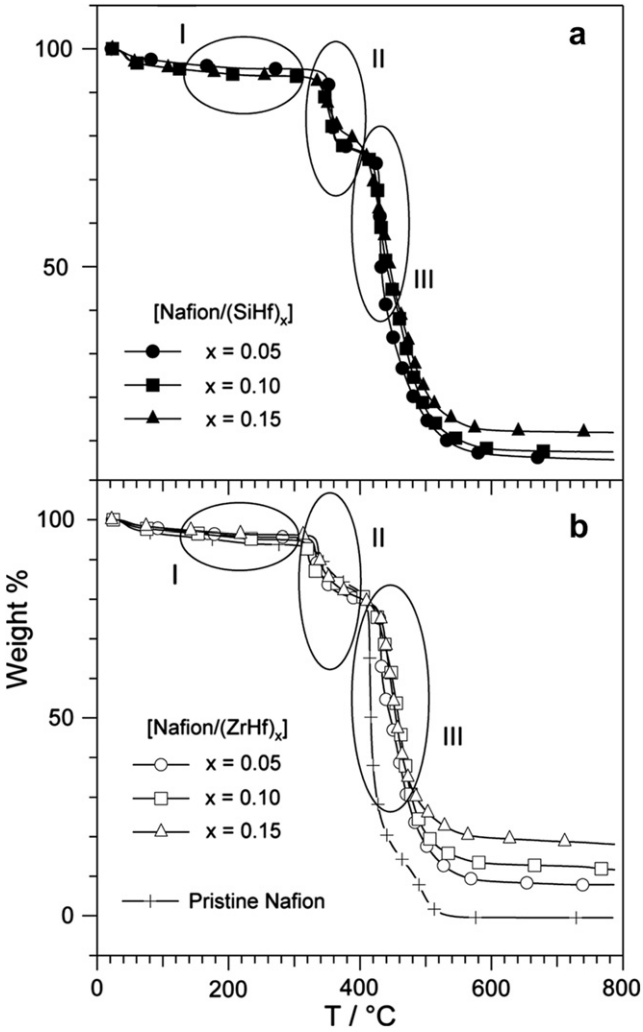

Fig. 5 – Thermogravimetric measurements of hybrid [Nafion/(ZrHf)$_x$] and [Nafion/(SiHf)$_x$] membranes; I, II and III indicate the main thermal degradation events.

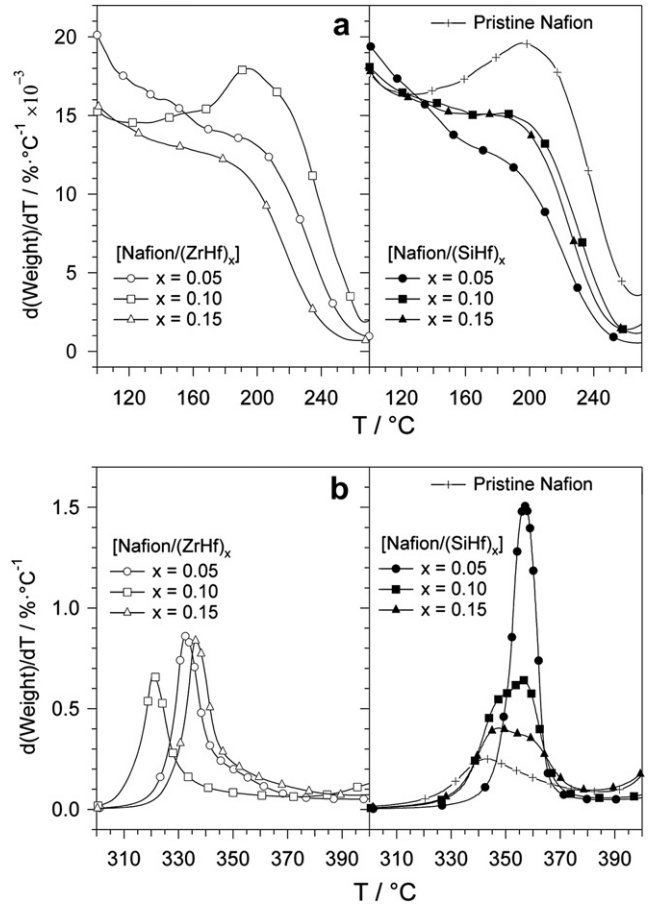

Fig. 6 – Derivatives of the TG profiles of hybrid [Nafion/(ZrHf)$_x$] and [Nafion/(SiHf)$_x$] membranes as a function of the temperature. (a) event I; (b) event II.

compared to pristine recast Nafion. The effect of the $[(ZrO_2)\cdot(HfO_2)_{0.25}]$ nanofiller on λ in [Nafion/(ZrHf)$_x$] membranes is significantly lower at both high and low values of water activity.

3.4. *TGA analysis of the membranes*

Fig. 5 reports the TGA profiles of the hybrid [Nafion/(ZrHf)$_x$] and [Nafion/(SiHf)$_x$] membranes. The thermal decomposition events typically observed in hybrid inorganic–organic Nafion-based membranes are evident [35,39,41,42]. The main degradation processes are labelled I, II and III; a further small elimination can be seen at $T < 100$ °C and is ascribed to the desorption of residual water from the membranes. Degradation I occurs between 100 and 250 °C and is attributed to the loss of the $-SO_3H$ groups of the Nafion host polymer. Degradation II is observed between 300 and 380 °C and originates in the decomposition of the perfluoroether side chains of Nafion. Finally, degradation III is evident at $T > 400$ °C and is due to the decomposition of the perfluorinated backbone chains of Nafion. The residue remaining at the highest temperatures ($T > 700$ °C) is in good agreement with the weight concentration of the inorganic nanofillers embedded in each hybrid membrane. Fig. 6 shows the derivatives of the TGA profiles reported in Fig. 5 in the temperature ranges from 100 to 270 °C (see Fig. 6(a)) and 300–400 °C (see Fig. 6(b)). Fig. 6(a) and (b) are intended to yield information about the thermal degradation events I and II, respectively. Fig. 6(a) reveals that a slightly lower loss of $-SO_3H$ groups occurs in the [Nafion/(ZrHf)$_x$] and [Nafion/(SiHf)$_x$] membranes than in pristine recast Nafion in the same temperature range. In contrast, Fig. 6(b) clearly indicates that the degradation of the perfluoroether side chains of the Nafion host polymer is quite different in the two families of hybrid membranes. Degradation II occurs at a temperature ca. 20 °C lower in all the [Nafion/(ZrHf)$_x$] membranes than in pristine recast Nafion. The opposite trend is found in the [Nafion/(SiHf)$_x$] membranes, where degradation II is manifested at temperatures ca. 20 °C higher in comparison to pristine recast Nafion. These results confirm that the catalytic effect of transition metal oxides on the polyether side group degradation of membranes is greater in [Nafion/(ZrHf)$_x$] than in [Nafion/(SiHf)$_x$].

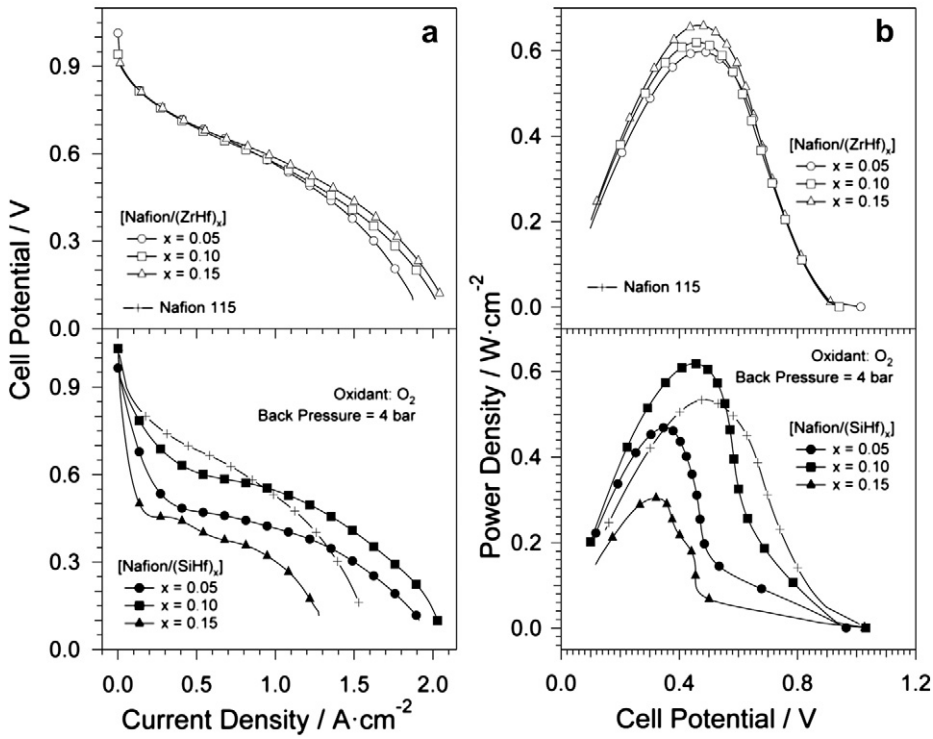

Fig. 7 – (a) Polarization curves; and (b) power curves of MEAs assembled with: a Nafion 115 membrane (+); the [Nafion/(ZrHf)$_x$] hybrid membranes (open symbols); the [Nafion/(SiHf)$_x$] hybrid membranes (solid symbols). The oxidant is pure oxygen and the back pressure is 4 bar at $a_{H2O} = 1$.

3.5. *Tests in a single-cell configuration*

3.5.1. *Single-cell performance at 4 bar and 100% RH*

Fig. 7 depicts the polarization and the power curves of MEAs assembled with Nafion 115, [Nafion/(ZrHf)$_x$] and [Nafion/(SiHf)$_x$] membranes in "ideal" operating conditions, i.e. using pure oxygen as the oxidant and fully-humidified reagent streams at a back pressure of 4 bar. The two families of proton-conducting materials are characterized by significantly different behaviours. As in the Nafion 115 reference membrane, the [Nafion/(ZrHf)$_x$] hybrid membranes feature polarization curves with a very similar S-shape. This shape originates from: (a) a sharp drop at the highest cell potentials, which essentially arises from the limited effectiveness of the cathode electrode due to the sluggishness of the oxygen reduction reaction; (b) a linear section at intermediate cell potentials, where the slope depends mainly on the various ohmic losses; and (c) a further drop at the lowest cell potentials as the limitations due to mass transport issues become progressively more important [3,5]. The initial potential drop of all the [Nafion/(ZrHf)$_x$] hybrid membranes is very similar to the Nafion 115 reference membrane. In comparison, in [Nafion/(SiHf)$_x$] hybrid membranes this initial drop is much more pronounced and continues up to current densities as high as 0.2–0.5 A cm^{-2}. In all the investigated MEAs, the slope of the linear section of the polarization curves is slightly lower than in the Nafion 115 reference. Finally, the polarization curves of all the MEAs, i.e. the Nafion 115 reference, the [Nafion/(ZrHf)$_x$] and the [Nafion/(SiHf)$_x$] hybrid membranes, show a similar trend at the lowest cell potentials. The difference in the initial potential drop of the polarization curves of the Nafion 115 reference and the [Nafion/(ZrHf)$_x$] hybrid membranes as compared to the [Nafion/(SiHf)$_x$] hybrid membranes is explained as follows. In the Nafion 115 reference and all the [Nafion/(ZrHf)$_x$] hybrid membranes, the initial portion of the polarization curve is controlled mainly by the electrode processes, particularly the oxygen reduction reaction [3,5,48]. It should be highlighted that: (a) all the MEAs mount gas-diffusion electrodes (GDEs) prepared with the same porous materials; (b) all the GDEs bear electrocatalytic layers sharing the same formulation and using the same functional materials (ionomer and electrocatalysts); and (c) all the MEAs are assembled according to the same protocol. Thus, since the Nafion 115 reference and the [Nafion/(ZrHf)$_x$] hybrid membranes mount the same electrodes, the initial portions of the polarization curves are essentially coincident as the ohmic contributions are assumed to be practically the same. In contrast, the initial potential drop in the polarization curves of all the [Nafion/(SiHf)$_x$] hybrid membranes is too large to be ascribed only to the sluggishness of the electrode processes. A significant contribution is expected to derive from ohmic losses. The latter mainly occurs due to: (a) the ohmic resistance of the membrane; (b) the ohmic resistances of the other components of the MEA; and (c) the resistance arising from the interfaces between the various layers of the MEA [3,5,48]. Contributions (b) and (c) are expected to be the

same for all the MEAs described in this report for the same reasons mentioned above. Therefore, the ohmic resistance of the proton-conducting membrane is assumed to be the discriminating factor. At low current densities, the ohmic resistance of the [Nafion/(SiHf)$_x$] hybrid membranes is expected to be very high, which leads to the observed steep potential drop. As the current density becomes larger than $J > 0.2–0.5$ A cm^{-2}, the proton conductivity of the membrane increases suddenly, leading to a significant decrease in the slope of the polarization curve. This event is interpreted by considering that as the current density of a fuel cell is raised, an increasing amount of water is obtained at the cathode as the final product of the overall reaction [1]. Thus, to operate properly the [Nafion/(SiHf)$_x$] hybrid membranes require more water than is provided by the reagent streams. The proton conductivity is increased only in these conditions. It is well-known that the slope of the I–V polarization curve of a MEA is a first approximation of its overall ohmic resistance, assuming that the cell potential: (a) is low enough to disregard contributions arising from electrode kinetics; and (b) no losses due to mass transport issues are observed [3,5,48]. In general, these conditions are satisfied in the linear section of a polarization curve located at intermediate cell potentials. The slopes of all the linear sections of the polarization curves of both the [Nafion/(ZrHf)$_x$] and [Nafion/(SiHf)$_x$] membranes are lower than in the Nafion 115 reference. In addition, the thickness of all the membranes presented in this report is comparable (ca. 110 μm). Therefore, it can be concluded that the proton conductivity of all the hybrid membranes is larger than the Nafion 115 reference, provided that their level of hydration is sufficiently high. In general, the mass transport issues affecting the shape of the polarization curve of a MEA depend on: (a) the features of the porous materials of the GDEs supporting the electrocatalytic layers; (b) the characteristics of the materials included in the electrocatalytic layers; (c) the formulation of the electrocatalytic layers; and (d) the operating conditions [3,5,48]. Since these points are the same for all the MEAs presented in this study, all of the polarization curves are affected by essentially the same mass transport issues, as is evident in the data reported in Fig. 7(a). Fig. 7(b) reports the power curves derived from Fig. 7(a) by plotting the current density versus the cell voltage. One way to gauge the overall performance of a MEA is to consider the maximum power density it can yield. In general, this maximum is located at potentials (current densities) which are: (a) high enough (low enough) to disregard the contributions arising from mass transport issues; and (b) low enough (high enough) to consider the electrode losses constant. These conditions are usually satisfied in the linear section of the polarization curve of a MEA, exactly where the ohmic contribution of the proton-conducting membrane plays the most important discriminating role. This is especially true in a series of MEAs assembled with the same procedure and using electrodes sharing the same formulation as in this report. Thus, it can be concluded that the maximum of the power density curve is an especially effective figure of merit to compare the overall performance of a series of similar MEAs.

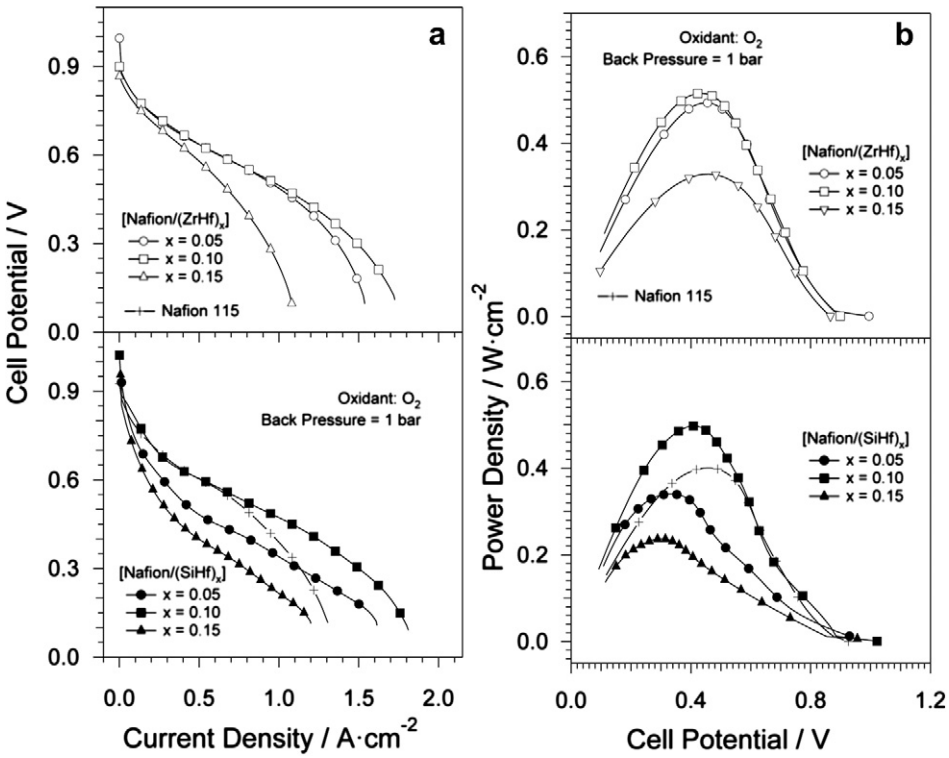

Fig. 8 – (a) Polarization curves; and (b) power curves obtained from MEAs assembled with: a Nafion 115 membrane (+); the [Nafion/(ZrHf)$_x$] hybrid membranes (open symbols); the [Nafion/(SiHf)$_x$] hybrid membranes (solid symbols). The oxidant is pure oxygen and the back pressure is 1 bar at $a_{H2O} = 1$.

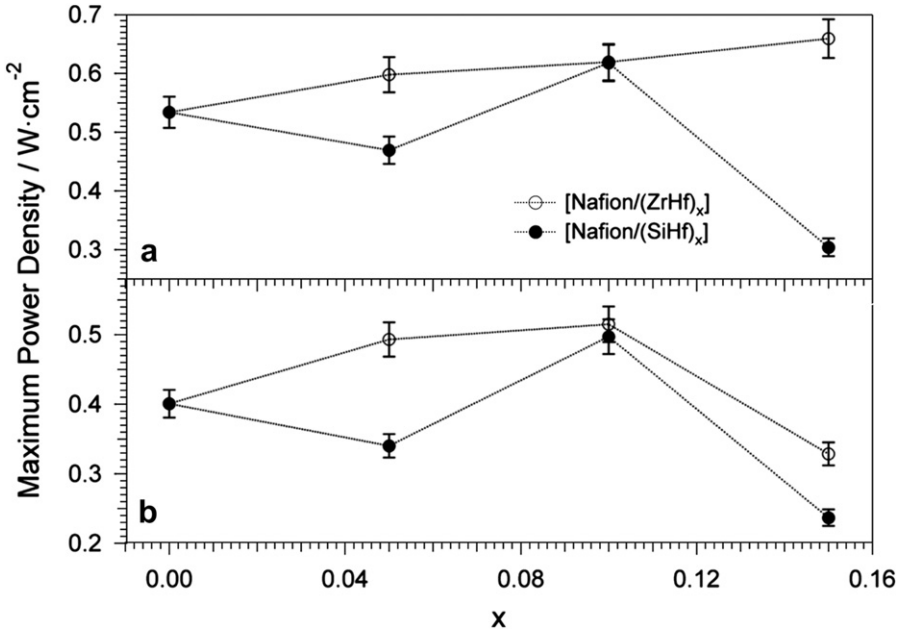

Fig. 9 – Dependence of the maxima of the power density on x. Data derived from Figs. 7 and 8. The oxidant is pure oxygen and the back pressure at a_{H2O} = 1 is: (a) 4 bar; (b) 1 bar.

3.5.2. *Single-cell performance at 1 bar and 100% RH*

Fig. 8 reports the polarization and power curves of all the MEAs, where the back pressure of the reagents is set at 1 bar. It is observed that the general trends highlighted in Fig. 7 are still very evident. In particular, the polarization curves of the [Nafion/$(ZrHf)_x$] hybrid membranes are very similar to those of the Nafion 115 reference. In contrast, the polarization curves of the [Nafion/$(SiHf)_x$] hybrid membranes show the same steep potential drop at high cell potentials, followed by a linear section showing essentially the same slope as the Nafion 115 reference. Finally, the contributions arising from mass transport issues are essentially the same for all the MEAs, i.e. the Nafion 115 reference, the [Nafion/$(ZrHf)_x$] and the [Nafion/$(SiHf)_x$] hybrid membranes. One major difference is highlighted between the data collected at different back pressures of the reagents. At a back pressure of 4 bar, the best polarization curve is found with the [Nafion/$(ZrHf)_{0.15}$] hybrid membrane, while at a back pressure of 1 bar, the same hybrid membrane is characterized by the worst polarization curve in its family and is much worse than the Nafion 115 reference.

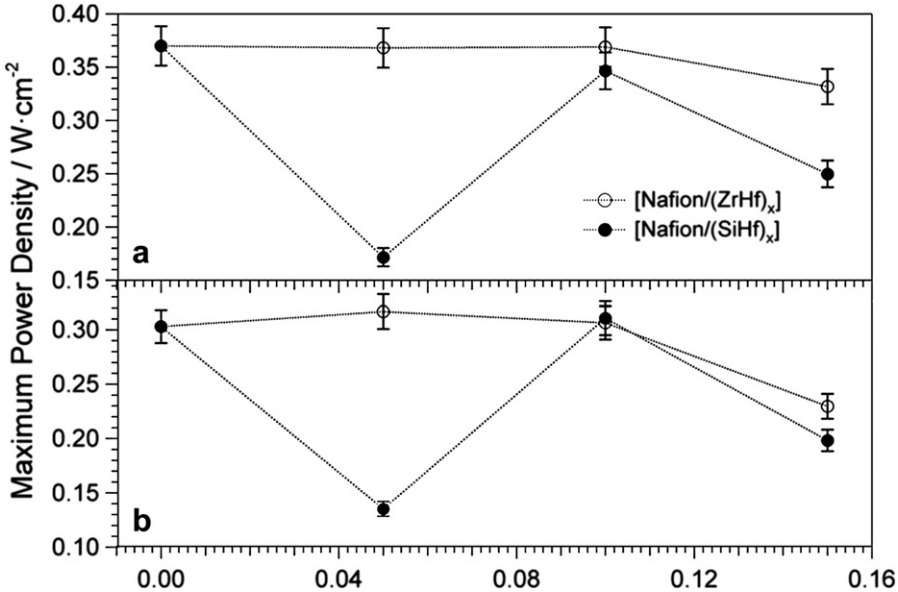

Fig. 10 – Dependence of the maxima of the power density on x. Data derived from Fig. S1 and Fig. S2 (see Supplementary Information). The oxidant is air and the back pressure at a_{H2O} = 1 is: (a) 4 bar; (b) 1 bar.

3.5.3. *Effect of nanofiller concentration on single-cell performance*

Figs. 9 and 10 show the maximum of the power density curves as a function of the mass fraction of nanofiller x using either pure oxygen or air as the oxidant, respectively. Fig. 9(b) clearly shows that the performance of [Nafion/$(ZrHf)_x$] hybrid membranes improves as the mass fraction of the nanofiller increases and is always better in comparison with the Nafion 115 reference. The maximum power densities yielded by the [Nafion/$(ZrHf)_{0.15}$] hybrid membrane and the Nafion 115 reference are 0.66 and 0.53 W cm^{-2}, respectively. In comparison, the performance of [Nafion/$(SiHf)_x$] hybrid membranes peaks at $x = 0.10$, where it is equal to 0.62 W cm^{-2}; the other membranes yield lower values than the Nafion 115 reference. As the back pressure of the reagents is reduced to 1 bar (see Fig. 9(a)), the same overall trends are observed. The only difference is that the best performance is observed for the [Nafion/$(ZrHf)_{0.10}$] hybrid membrane, which yields a maximum power density equal to 0.52 W cm^{-2} versus 0.40 W cm^{-2} for the Nafion 115 reference. The performance of the [Nafion/$(ZrHf)_{0.15}$] membrane is significantly lower, as it yields a maximum of 0.33 W cm^{-2}. As for the [Nafion/$(SiHf)_x$] hybrid membranes, the best performance is obtained at $x = 0.10$, where the maximum power density is equal to 0.50 W cm^{-2}. The trends of the maxima of the power curves determined using air as the oxidant (see Fig. 10) are essentially the same as those with pure oxygen, previously reported in Fig. 8.

3.5.4. *Effect of water vapour activity on single-cell performance*

Figs. 11–13 show the envelopes of selected polarization and power curves determined for the Nafion 115 reference, the [Nafion/$(ZrHf)_{0.05}$] and the [Nafion/$(SiHf)_{0.05}$] hybrid membranes, respectively, as a function of the water vapour activity in the reagent streams. All the envelopes collected for the remaining membranes using both pure oxygen and air as the oxidant are reported in the Supplementary Information. It is observed that the overall performance of the membranes decreases as the a_{H2O} in the reagent streams decreases. Specifically, the shape of the polarization curves is altered and two main effects are evident: (a) a potential drop at high cell potentials; and (b) an increase in the slope of the linear section

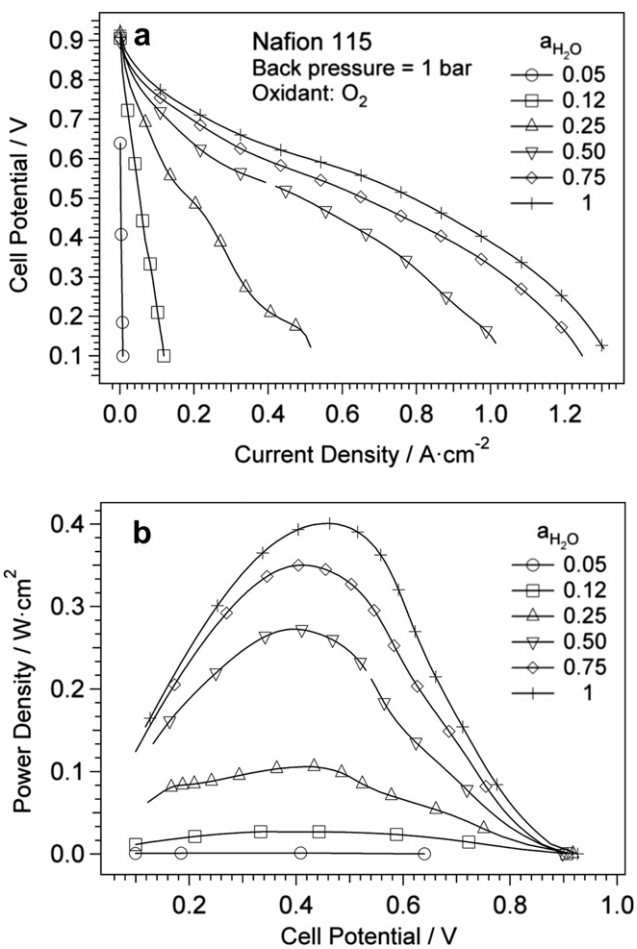

Fig. 11 – Envelope of: (a) the polarization curves; and (b) the power curves of the MEA assembled with the Nafion 115 membrane as a function of a_{H2O} in the reagent streams. The oxidant is pure oxygen and the back pressure is 1 bar.

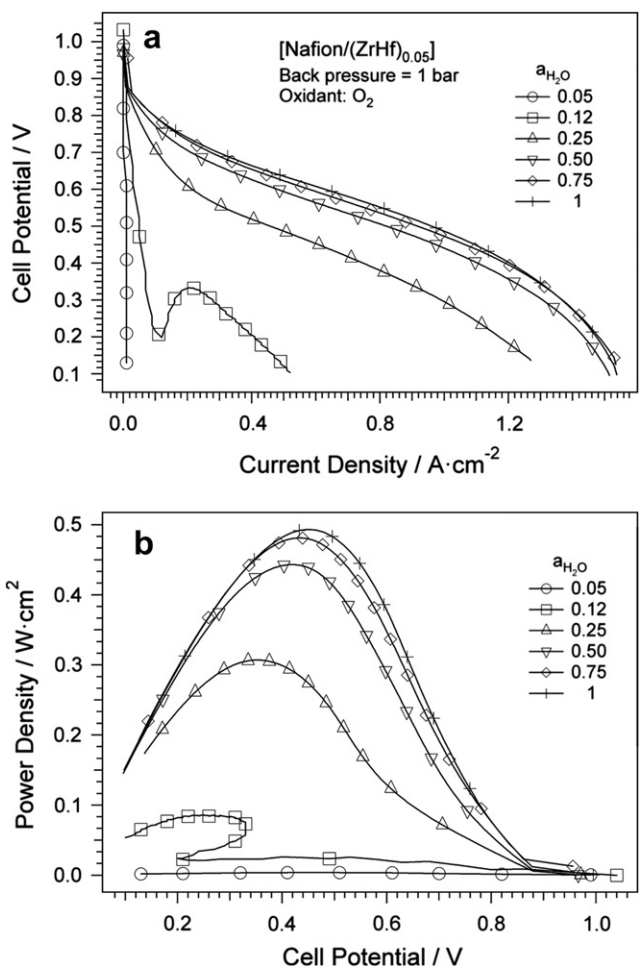

Fig. 12 – Envelope of: (a) the polarization curves; and (b) the power curves of the MEA assembled with the [Nafion/$(ZrHf)_{0.05}$] membrane as a function of a_{H2O} in the reagent streams. The oxidant is pure oxygen and the back pressure is 1 bar.

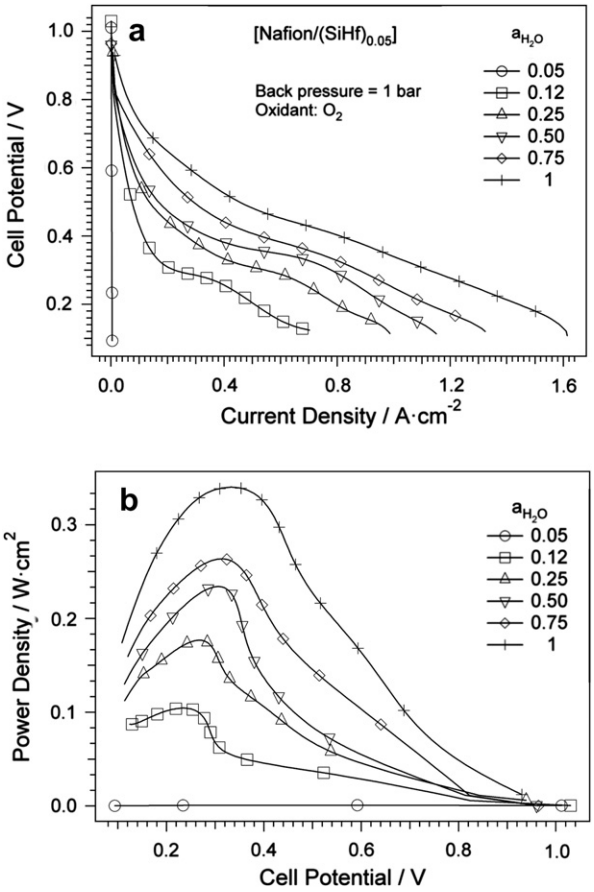

Fig. 13 – Envelope of: (a) the polarization curves; and (b) the power curves of the MEA assembled with the [Nafion/(SiHf)$_{0.05}$] membrane as a function of a_{H2O} in the reagent streams. The oxidant is pure oxygen and the back pressure is 1 bar.

of the polarization curves. It is not easy to quantify the relative importance of these two effects for each membrane at the different values of a_{H2O} in the reagent streams. However, it can be noted that the two effects tend to exclude one another. When a potential drop at high potentials is evident, the slope of the linear section of the polarization curve tends to be almost constant regardless of a_{H2O} in the reagent streams, as is the case in the [Nafion/(SiHf)$_{0.05}$] hybrid membrane (see Fig. 13(a)). In comparison, if the slope of the linear section of the polarization curves increases as a_{H2O} in the reagent streams decreases, very little potential drop generally is observed at the highest cell potentials as in the Nafion 115 reference (see Fig. 11(a)). Finally, the polarization curves collected using pure oxygen as the oxidant tend to preserve the slope of the linear section of the polarization curve regardless of a_{H2O} in the reagent streams (see the Supplementary Information) as compared to those using air as the oxidant. These results can be explained considering that the proton conductivity of all the membranes is not constant along the polarization curve. Rather, as the current density becomes larger than a certain threshold level, the MEA becomes self-humidified, i.e. the proton conductivity of its membrane increases markedly following an increased production of water as the reaction by-product. A rough estimate indicates that this threshold current density at a back pressure of 1 bar falls between ca. 0.15 and 0.3 A cm^{-2}. It is noted that in certain cases as the current density becomes larger than a threshold value the increase in the proton conductivity is sudden and very significant, as indicated by the marked "bump" in the polarization curve of the [Nafion/(ZrHf)$_{0.05}$] hybrid membrane where a_{H2O} in the reagent streams is 0.12 (see Fig. 12(a)). In this case, the effect is so evident that the cell voltage actually increases from 0.2 to 0.35 V as the current density is increased from 0.12 to 0.22 A cm^{-2}. When the cathode electrode is fed with pure oxygen, it operates more effectively than when it is fed with air, leading to higher cell potentials at the same current densities [3,5,48]. As a direct consequence, the same MEA becomes more easily self-humidified when it is fed with pure oxygen because it is able to support larger current densities and consequently produces more water. This explains why polarization curves for MEAs fed with pure oxygen tend to conserve the slope of the linear portion of the polarization curve regardless of a_{H2O} in the reagent streams. Fig. 14 reports

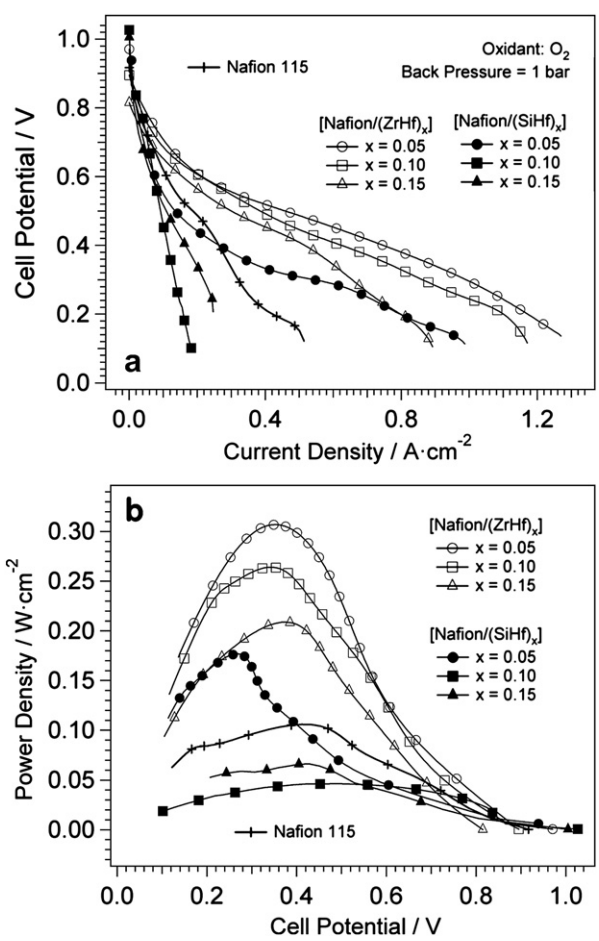

Fig. 14 – (a) Polarization curves; and (b) power curves of MEAs assembled with: a Nafion 115 membrane (+); the [Nafion/(ZrHf)$_x$] hybrid membranes (open symbols); the [Nafion/(SiHf)$_x$] hybrid membranes (solid symbols). The oxidant is pure oxygen and the back pressure is 1 bar at a_{H2O} = 0.25.

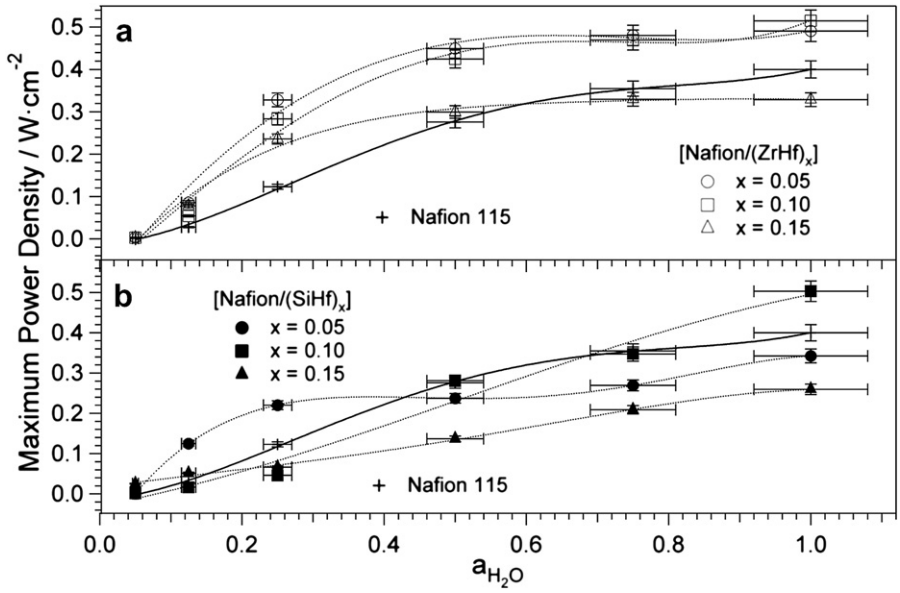

Fig. 15 – Dependence on a_{H2O} of the maxima of power curves for: (a) [Nafion/(ZrHf)$_x$]; and (b) [Nafion/(SiHf)$_x$] hybrid membranes. The oxidant is pure oxygen and the back pressure is 1 bar. The lines are meant as a guide for the eye.

the polarization and the power curves of the hybrid membranes and the Nafion 115 reference where a_{H2O} in the reagent streams is 0.25. It is observed clearly that the performance of the [Nafion/(ZrHf)$_x$] hybrid membranes is higher than the Nafion 115 reference and improves as the weight fraction of the nanofiller x decreases from 0.15 to 0.05. For the [Nafion/(SiHf)$_x$] hybrid membranes, it is noted that if $x = 0.05$ the membrane becomes self-humidified at a current density of ca. 0.2 A cm^{-2}, yielding a higher performance in comparison with the Nafion 115 reference. However, if $x = 0.10$ or $x = 0.15$, no such self-humidification is registered and the performance of the membranes drops well below the level typical of the reference. Fig. 15 reports the maxima of the power density curves obtained for each membrane as a function of a_{H2O} in the reagent streams as they are fed with pure oxygen. Fig. 16 shows the corresponding data for systems fuelled with air at the cathode. In both cases it is observed that the performance of the [Nafion/(ZrHf)$_x$] membranes is superior than in the Nafion 115 reference, especially if a_{H2O} in the reagent streams is lower than 0.5. For example, at $a_{H2O} = 0.25$ and fuelling the MEAs with pure oxygen, the maximum power densities obtained from the [Nafion/(ZrHf)$_{0.05}$] and the Nafion 115

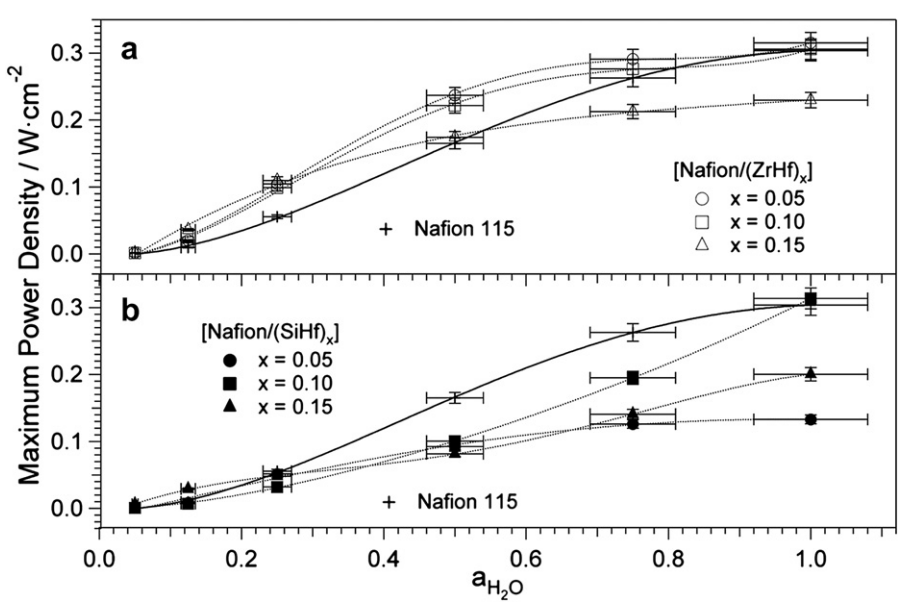

Fig. 16 – Dependence on a_{H2O} of the maxima of power curves for: (a) [Nafion/(ZrHf)$_x$]; and (b) [Nafion/(SiHf)$_x$] hybrid membranes. The oxidant is air and the back pressure is 1 bar. The lines are meant as a guide for the eye.

reference are 0.31 and 0.11 W cm^{-2}, respectively. In contrast, the performance of the [Nafion/$(SiHf)_x$] membranes is significantly worse than the Nafion 115 reference. The performance of [Nafion/$(SiHf)_x$] is more significantly affected as a_{H2O} in the reagent streams is lowered below 1. It is also evident that the general trends highlighted in Fig. 15 concerning the performance of all the membranes fuelled with pure oxygen are not altered significantly when the membranes are fuelled with air as indicated by Fig. 16. In general, it is revealed that the relative performance of the various membranes is not affected significantly by a_{H2O} in the reagent streams. In other words, if the performance of a given membrane is higher with respect to any other at $a_{H2O} = 1$, the same relative order is conserved for all the other values of a_{H2O}. The most evident exception to this general trend occurs in the [Nafion/$(SiHf)_{0.05}$] hybrid membrane when it is fuelled with pure oxygen (see Fig. 15(b)), where the performance becomes significantly higher in comparison with the Nafion 115 reference at $0.12 \leq a_{H2O} \leq 0.25$.

4. Discussion

The data presented in this work can be rationalized in a coherent picture by considering the Nafion-nanofiller interactions occurring due to the presence of the nanofiller particles in the structure of pristine Nafion. It is well-known that Nafion is characterized by hydrophilic domains dispersed in a highly hydrophobic matrix [10]. Water is absorbed in the hydrophilic domains, where it causes the dissociation of the $-SO_3H$ groups found at the domain boundaries [49]. Thus, H_3O^+ ions are produced and quickly diffuse within each hydrophilic domain [50,51]. However, the long-range migration of the protons is only possible when two different hydrophilic domains come into contact following the relaxation of the hydrophobic matrix [11,34]. The hydrophobic domains include fluorocarbon helices characterized by at least two main conformations: 15_7 and 10_3. The 15_7 conformation is largely dominant and gives rise to highly ordered polymeric "bundles". The 10_3 conformation gives rise to a much more disordered local structure [52]. In a hybrid inorganic–organic Nafion-based material, the addition of the nanofiller particles alters this picture. The development of dynamic cross-links between the nanofiller particles and the Nafion host polymer is signified by a significant improvement in the mechanical properties of the hybrid materials over pristine Nafion, especially at $T > 100$ °C [36,38–41,53]. It is widely reported that these dynamic cross-links may take place between the $-SO_3H$ groups of the Nafion host polymer and the surface of the nanofiller particles [36,38,39,41]. The secondary structure of the Nafion host polymer is also significantly affected. In hybrid inorganic–organic Nafion-based materials, the concentration of the fluorocarbon helices characterized by the 10_3 conformation increases markedly as compared to pristine Nafion [39]. In the [Nafion/$(ZrHf)_x$] and [Nafion/$(SiHf)_x$] hybrid membranes studied here, it is observed that the nanofiller particles interact with the $-SO_3H$ groups of the Nafion host polymer. Fig. 6(a) clearly shows that in both the [Nafion/$(ZrHf)_x$] and [Nafion/$(SiHf)_x$] hybrid membranes, as compared to pristine Nafion, the decomposition of the $-SO_3H$ groups is inhibited by the stabilizing effect introduced by interaction with the nanofiller particles. In contrast the decomposition of the perfluoroether side chains of the Nafion host polymer in the [Nafion/$(ZrHf)_x$] hybrid membranes occurs at a temperature ca. 20 °C lower than in pristine Nafion. The opposite trend is observed in the [Nafion/$(SiHf)_x$] hybrid membranes. This evidence is interpreted considering that in [Nafion/$(ZrHf)_x$] hybrid membranes the Nafion-nanofiller interactions destabilize the perfluoroether side chains of the Nafion host polymer, while the opposite occurs in [Nafion/$(SiHf)_x$] hybrid membranes. Recall that the perfluoroether side chains are located at the interface between the hydrophilic and the hydrophobic domains of the Nafion host polymer. Therefore, strong Nafion-nanofiller interactions promote the thermal degradation of the perfluoroether side chains and enhance the coupling phenomena between the relaxation events of the two domains. Consequently, in [Nafion/$(ZrHf)_x$] hybrid membranes the hydrophilic domains are assumed to be less mobile than in pristine Nafion, while the opposite would occur in [Nafion/$(SiHf)_x$] hybrid membranes. Thus, the addition of $[(ZrO_2))\cdot(HfO_2)_{0.25}]$ and $[(SiO_2)\cdot(HfO_2)_{0.28}]$ nanofiller is expected to alter significantly the ordering of the perfluorinated backbone chains, triggering the $15_7 \rightarrow 10_3$ conformational transition. An increased concentration of 10_3 helices in both the [Nafion/$(ZrHf)_x$] and the [Nafion/$(SiHf)_x$] would be consistent with the larger water uptake in comparison with the pristine Nafion both at high and low values of the water vapour activity (see Figs. 3 and 4). This latter result is in line with other evidence found in the literature [39] and is ascribed to the higher water uptake associated with the solvation phenomena of Nafion-nanofiller cross-links. The solvation phenomena are expected to become more significant as the strength of the Nafion-nanofiller cross-links increases, i.e. as the ionic character of the Nafion-nanofiller becomes higher. Therefore, the protons of the $-SO_3H$ groups of the Nafion host polymer are assumed to be delocalized over the surface of the $[(ZrO_2)\cdot(HfO_2)_{0.25}]$ particles owing to the stronger interactions in [Nafion/$(ZrHf)_x$] membranes. The difference in the interactions between the $-SO_3H$ groups of the Nafion host polymer and the nanofiller particles in the two families of hybrid membranes is ascribed to the acid–base properties of the surface of the latter component. It is well-known that the basic character of the oxides studied in this work increases as follows: $SiO_2 << ZrO_2 < HfO_2$ [28]. Thus, the surface of the $[(ZrO_2)\cdot(HfO_2)_{0.25}]$ nanofiller is expected to be much more basic than the surface of the $[(SiO_2)\cdot(HfO_2)_{0.28}]$ nanofiller. The $[(ZrO_2)\cdot(HfO_2)_{0.25}]$ nanofiller is capable of triggering the formation of $-SO_3^-\cdots\{[(ZrO_2)\cdot(HfO_2)_{0.25}]\cdot H\}^+$ bridges owing to non-directional ionic interactions, while the $[(SiO_2)\cdot(HfO_2)_{0.28}]$ nanofiller can only give rise to localized and highly directional $-SO_3H\cdots[(SiO_2)\cdot(HfO_2)_{0.28}]$ dipolar interactions (see Figs. 1 and 2). The relatively poor fuel cell performance of the [Nafion/$(SiHf)_{0.05}$] hybrid membrane is ascribed to the low delocalization of protons. In this case the protons of the Nafion $-SO_3H$ groups tend to be localized in direct interactions with the nanofiller particles. In comparison, the fuel cell performance of [Nafion/$(SiHf)_{0.10}$] hybrid membrane is significantly improved. This evidence indicates that the introduction of a larger mass fraction of nanofiller promotes the structural

disorder of the Nafion host polymer, thus promoting the proton delocalization in bulk membranes. Taken together, the proton localization at the Nafion-nanofiller interfaces hinders the conductivity of the membranes. The maximum performance is achieved only as the reagent streams are fully humidified and only when additional water is produced by the cell during operation as the output current density becomes larger than 0.3–0.5 A cm^{-2} (see Fig. 7). In these conditions, the [Nafion/$(SiHf)_{0.10}$] hybrid membrane probably is capable of holding more water than the Nafion 115 reference, yielding wider proton-conducting channels. This hypothesis is also consistent with the data shown in Figs. 3 and 4. In these conditions, the [Nafion/$(SiHf)_{0.10}$] hybrid membrane reaches a higher proton conductivity than the Nafion 115 reference as signified by the lower slope of the polarization curve in its linear section at a current density of 0.5–1 A cm^{-2} (see Fig. 7). In the case of the [Nafion/$(SiHf)_{0.15}$] hybrid membrane, a drop in fuel cell performance is observed in comparison with the other membranes of this family. The formation of nanofiller aggregates results in nanofiller–nanofiller interfaces unable to promote proton delocalization in bulk membranes. Thus, the proton conductivity of the [Nafion/$(SiHf)_{0.15}$] hybrid membrane is reduced, since: (a) the protons have to travel around the water solvation shells of aggregates with a low basic character; and (b) the formation of a higher concentration of filler aggregates acts to dilute the density of charge carriers. These results are in agreement with the morphological studies carried out by HR-TEM. The fuel cell performance of [Nafion/$(ZrHf)_{0.05}$] and [Nafion/$(ZrHf)_{0.10}$] hybrid membranes is markedly improved as compared to the Nafion 115 reference because the mobility of the protons in the hydrophilic domains is higher. In this case, the proton is delocalized on the surface of the $[(ZrO_2)\cdot(HfO_2)_{0.25}]$ nanofiller owing to the strength of the $-SO_3^-\cdots\{[(ZrO_2)\cdot(HfO_2)_{0.25}]\cdot H\}^+$ cross-links. In addition, these interactions are responsible for the proton delocalization in bulk membranes through the water solvation shell of the Nafion-nanofiller cross-links. The performance increases as the mass fraction of the $[(ZrO_2)\cdot(HfO_2)_{0.25}]$ nanofiller x increases up to 0.1 because the density of Nafion-nanofiller cross-links increases. At $x > 0.1$ the performance is reduced owing to the formation of nanofiller–nanofiller aggregates, which act to dilute the concentration of charge carriers. This interpretation is also supported by the result that the [Nafion/$(ZrHf)_{0.15}$] hybrid membrane shows the highest performance for all the materials discussed in this work if it is fuelled with pure oxygen and fully-humidified reagent streams at a back pressure of 4 bar (see Fig. 7). Thus, the presence of a high water content in the hydrophilic domains of the hybrid membranes facilitates the long-range proton migration. In these conditions and as the cell produces high current densities, the highest power density, i.e. 0.66 W cm^{-2}, recorded in this work is achieved. This evidence indicates that the interfaces between the particles of the $[(ZrO_2)\cdot(HfO_2)_{0.25}]$ nanofiller may become capable of carrying protons effectively only if the hydration level of the membrane becomes larger than a certain threshold. The proton conductivity of the hybrid membrane is increased in these conditions, therefore enhancing the maximum power density yielded by the fuel cell. These results suggest that a suitable hydration level is necessary to form a continuous solvation shell around Nafion-nanofiller cross-links, which facilitates the long-range charge transfer process. This condition is reached if the fuel cell produces a sufficiently high current density and consequently a large amount of water as the reaction product. The fuel cell performance of [Nafion/$(ZrHf)_x$] hybrid membranes is significantly improved, as compared to the Nafion 115 reference and the [Nafion/$(SiHf)_x$] hybrid membranes, even when a_{H2O} in the reagent streams is low (see Figs. 14–16). This evidence is easily interpreted in the proposed framework describing the effect of the nanofiller on the structure and proton conductivity mechanism of these families of hybrid inorganic–organic materials. Indeed, as compared to the Nafion 115 reference: (a) the water uptake of both the [Nafion/$(SiHf)_x$] and the [Nafion/$(ZrHf)_x$] hybrid membranes is higher in these conditions and is correlated to the density of Nafion-nanofiller cross-links (see Figs. 3 and 4); and (b) the factor responsible for the improved proton mobility in the hydrophilic domains is the basicity of the $[(ZrO_2)\cdot(HfO_2)_{0.25}]$ nanofiller, which improves the strength of the Nafion-nanofiller cross-links and facilitates the proton delocalization in the hydrophilic domains of the hybrid membranes in the presence of solvation water. The final result is an improved proton conductivity of the [Nafion/$(ZrHf)_x$] hybrid membranes even at low hydration degrees.

5. Conclusions

In this work, two "core–shell" nanofillers are obtained by grinding either SiO_2 or ZrO_2 with HfO_2. The resulting $[(ZrO_2)\cdot(HfO_2)_{0.25}]$ and $[(SiO_2)\cdot(HfO_2)_{0.28}]$ nanofillers are used in the preparation of two families of three hybrid inorganic–organic membranes each. Nafion is used as the host polymer, and the mass fraction of nanofiller x is set as 0.05, 0.10 and 0.15. The membranes are obtained with a solvent-casting procedure and are subsequently purified and activated. The nanofillers do not provide additional contributions to the nominal proton exchange capacity of the hybrid membranes, as indicated by titration measurements. It is demonstrated that the water uptake of both [Nafion/$(ZrHf)_x$] and [Nafion/$(SiHf)_x$] hybrid membranes is larger than pristine Nafion both at high and at low values of activity of water vapour in the environment. Thermogravimetric measurements show that the addition of nanofiller stabilizes the $-SO_3H$ groups of the Nafion host polymer. In contrast, the interactions between the nanofiller and the polymer matrix stabilize the perfluoroether side chains of the Nafion host polymer in [Nafion/$(SiHf)_x$] hybrid membranes. The opposite trend is observed in [Nafion/$(ZrHf)_x$] hybrid membranes. The fuel cell performance of [Nafion/$(SiHf)_x$] hybrid membranes is lower than the [Nafion/$(ZrHf)_x$] hybrid membranes at both high and low water vapour activities in the reagent streams. In general, the best performance of both families of membranes is obtained at $x = 0.10$. As the fuel cells are fed with fully-humidified reagent streams at a back pressure of 1 bar and using pure oxygen as the oxidant, the maximum power density yielded by the Nafion 115 reference, the [Nafion/$(ZrHf)_{0.10}$] and the [Nafion/$(SiHf)_{0.10}$] hybrid membranes is 0.40, 0.52 and 0.50 W cm^{-2}, respectively. As a_{H2O} in the reagent streams is lowered, the fuel cell performance of all the

membranes is significantly compromised. However, it is observed that this effect increases in the order [Nafion/$(ZrHf)_x$] hybrid membranes < Nafion 115 reference < [Nafion/$(SiHf)_x$] hybrid membranes. In particular, at $a_{H2O} = 0.25$, with the back pressure of the reagents set to 1 bar and using pure oxygen as the oxidant, the maximum power density yielded by [Nafion/$(ZrHf)_{0.10}$] hybrid membrane, Nafion 115 reference and [Nafion/$(SiHf)_{0.10}$] is 0.26, 0.11 and 0.05 W cm^{-2}, respectively. The data are rationalized taking into account: (a) the modifications of the secondary structure of the Nafion host polymer upon the introduction of the nanofiller particles; and (b) the interactions between the nanofiller particles and the $-SO_3H$ groups of the Nafion host polymer. The presence of the nanofillers in the hybrid membranes increases the concentration of the 10_3 helical conformation of the Nafion host polymer, which improves the Nafion-nanofiller interactions. The strength of these interactions depends on the basicity of the nanofiller. The density and the strength of the Nafion-nanofiller cross-links increase from [Nafion/$(SiHf)_x$] to [Nafion/$(ZrHf)_x$] hybrid membranes with the increase in the ionic character of the Nafion-nanofiller interactions. Therefore, it is proposed that in the membranes based on the $[(ZrO_2)\cdot(HfO_2)_{0.25}]$ nanofiller the bulk conductivity is enhanced owing to the efficient delocalization of the protons, which is promoted by the Nafion-nanofiller interfaces. The opposite phenomena occur in the [Nafion/$(SiHf)_x$] hybrid membranes, where the Nafion-nanofiller interactions take place according to a dipolar mechanism that acts to reduce the delocalization of the protons.

Acknowledgements

Research was funded by the Italian MURST project PRIN2007, “Passive direct methanol fuel cells: electrocatalysts for the oxygen reduction reaction based on carbon nitride supports and hybrid inorganic–organic membranes based on fluorinated ionomers and nanoparticles of mixed oxoclusters”. The author N. B. thanks Texa S.p.A. for the Ph. D. grant. The authors extend their most sincere thanks to the staff of the mechanical workshop of the Department of Chemical Sciences of the University of Padova for the skillful technical assistance, provided by Mr. Stefano Mercanzin, Mr. Roberto Inilli, Mr. Vincenzo Afelbo, Mr. Lorenzo Dainese and Mr. Paolo Roverato.”

Appendix. Supplementary material

Supplementary data associated with this article can be found, in the online version, at doi:10.1016/j.ijhydene.2011.07.132.

REFERENCES

[1] Vielstich W. Ideal and effective efficiencies of cell reactions and comparison to Carnot cycles. In: Vielstich W, Lamm A, Gasteiger HA, editors. Handbook of fuel cells: fundamentals technology and applications, vol. 1. Chichester: John Wiley & Sons; 2003. p. 26–30.
[2] Larminie J, Dicks A. Fuel cell systems explained. John Wiley & Sons; 2003.
[3] Srinivasan S. Fuel cells - from fundamentals to applications. New York: Springer Science; 2006.
[4] Peighambardoust SJ, Rowshanzamir S, Amjadi M. Review of the proton exchange membranes for fuel cell applications. Int J Hydrogen Energy 2010;35:9349–84.
[5] O'Hayre R, Cha SW, Colella W, Prinz FB. Fuel cell fundamentals. New York: John Wiley & Sons; 2006.
[6] Kreuer KD. Hydrocarbon membranes. In: Vielstich W, Lamm A, Gasteiger HA, editors. Handbook of fuel cells: fundamentals technology and applications, vol. 3. Chichester: John Wiley & Sons; 2003. p. 420–35.
[7] Alberti G, Casciola M. Composite membranes for medium-temperature PEM fuel cells. Annu Rev Mat Res 2003;33: 129–54.
[8] Sgreccia E, Di Vona ML, Knauth P. Hybrid composite membranes based on SPEEK and functionalized PPSU for PEM fuel cells. Int J Hydrogen Energy 2011;36:8063–9.
[9] Grot W. Fluorinated ionomers. Norwich: William Andrew Inc; 2008.
[10] Mauritz KA, Moore RB. State of understanding of Nafion. Chem Rev 2004;104:4535–85.
[11] Di Noto V, Negro E, Lavina S. Broadband dielectric spectroscopy and conductivity mechanism of Nafion 117 and Nafion/[ZrO_2] hybrid inorganic-organic membranes. In: Herring AM, Zawodzinski TA, Hamrock SJ, editors. ACS symposium series. Fuel cell chemistry and operation, vol. 1040. Washington, DC: ACS Publications; 2010. p. 219–77.
[12] Doyle M, Rajendran G. Perfluorinated membranes. In: Vielstich W, Lamm A, Gasteiger HA, editors. Handbook of fuel cells: fundamentals technology and applications, vol. 3. Chichester: John Wiley & Sons; 2003. p. 391–5.
[13] Borup R, Meyers J, Pivovar B, Kim YS, Mukundan R, Garland N, et al. Scientific aspects of polymer electrolyte fuel cell durability and degradation. Chem Rev 2007;107:3904–51.
[14] Rostrup-Nielsen JR, Aasberg-Petersen K. Steam-reforming, atr, partial oxidation: catalysts and reaction engineering. In: Vielstich W, Lamm A, Gasteiger HA, editors. Handbook of fuel cells: fundamentals technology and applications, vol. 3. Chichester: John Wiley & Sons; 2003. p. 159–76.
[15] Hidalgo-Vivas A, Cooper BH. Sulfur removal methods. In: Vielstich W, Lamm A, Gasteiger HA, editors. Handbook of fuel cells: fundamentals technology and applications, vol. 3. Chichester: John Wiley & Sons; 2003. p. 177–89.
[16] Aricò AS, Baglio V, Di Blasi A, Creti P, Antonucci PL, Antonucci V. Influence of the acid–base characteristics of inorganic fillers on the high temperature performance of composite membranes in direct methanol fuel cells. Solid State Ionics 2003;161:251–65.
[17] Aricò AS, Baglio V, Di Blasi A, Modica E, Antonucci PL, Antonucci V. Surface properties of inorganic fillers for application in composite membranes - direct methanol fuel cells. J Power Sources 2004;128:113–8.
[18] Thiam HS, Daud WRW, Kamarudin SK, Mohammad AB, Kadhum AAH, Loh KS, et al. Overview on nanostructured membrane in fuel cell applications. Int J Hydrogen Energy 2011;36:3187–205.
[19] Neergat M, Griedrich KA, Stimming U. New materials for DMFC MEAs. In: Vielstich W, Lamm A, Gasteiger HA, editors. Handbook of fuel cells: fundamentals technology and applications, vol. 4. Chichester: John Wiley & Sons; 2003. p. 856–77.
[20] Nakao M, Yoshitake M. Composite perfluorinate membranes. In: Vielstich W, Lamm A, Gasteiger HA, editors. Handbook of fuel cells: fundamentals technology and applications, vol. 4. Chichester: John Wiley & Sons; 2003. p. 412–9.

[21] Mauritz KA. Organic–inorganic hybrid materials: perfluorinated ionomers as sol–gel polymerization templates for inorganic alkoxides. Mater Sci Eng C 1998;6: 121–33.

[22] Honma I, Nakajima H, Nishikawa O, Sugimoto T, Nomura S. Organic/inorganic nano-composites for high temperature proton conducting polymer electrolytes. Solid State Ionics 2003;162–163:237–45.

[23] Jalani NH, Dunn K, Datta R. Synthesis and characterization of Nafion®-MO_2 (M = Zr, Si, Ti) nanocomposite membranes for higher temperature PEM fuel cells. Electrochim Acta 2005;51: 553–60.

[24] Jiang RC, Kunz HR, Fenton JM. Composite Silica/Nafion® membranes prepared by tetraethylorthosilicate sol-gel reaction and solution casting for direct methanol fuel cells. J Membr Sci 2006;272:116–24.

[25] Adjemian KT, Lee SJ, Srinivasan S, Benziger J, Bocarsly AB. Silicon oxide Nafion composite membranes for proton-exchange membrane fuel cell operation at 80–140 °C. J Electrochem Soc 2002;149:A256–61.

[26] Casciola M, Alberti G, Sganappa M, Narducci R. On the decay of Nafion proton conductivity at high temperature and relative humidity. J Power Sources 2006;162:141–5.

[27] Helen M, Viswanathan B, Murthy SS. Synthesis and characterization of composite membranes based on α-zirconium phosphate and silicotungstic acid. J Membr Sci 2007;292:98–105.

[28] Wang K, McDermid S, Li J, Kremliakova N, Kozak P, Song C, et al. Preparation and performance of nano silica/Nafion composite membrane for proton exchange membrane fuel cells. J Power Sources 2008;184:99–103.

[29] Neburchilov V, Martin J, Wang H, Zhang J. A review of polymer electrolyte membranes for direct methanol fuel cells. J Power Sources 2007;169:221–38.

[30] Chen SY, Han CC, Tsai CH, Huang J, Chen-Yang YW. Effect of morphological properties of ionic liquid-templated mesoporous anatase TiO_2 on performance of PEMFC with Nafion/TiO_2 composite membrane at elevated temperature and low relative humidity. J Power Sources 2007;171:363–72.

[31] Truffier-Boutry D, De GA, Guetaz L, Diat O, Gebel G. Structural study of zirconium phosphate-Nafion hybrid membranes for high-temperature proton exchange membrane fuel cell applications. Macromolecules 2007;40: 8259–64.

[32] Amjadi M, Rowshanzamir S, Peighambardoust SJ, Hosseini MG, Eikani MH. Investigation of physical properties and cell performance of Nafion/TiO_2 nanocomposite membranes for high temperature PEM fuel cells. Int J Hydrogen Energy 2010;35:9252–60.

[33] Pan J, Zhang H, Chen W, Pan M. Nafion-zirconia nanocomposite membranes formed via in situ sol–gel process. Int J Hydrogen Energy 2010;35:2796–801.

[34] Di Noto V, Gliubizzi R, Negro E, Pace G. Effect of SiO_2 on relaxation phenomena and mechanism of ion conductivity of [Nafion/$(SiO_2)_x$] Composite membranes. J Phys Chem B 2006;110:24972–86.

[35] Di Noto V, Gliubizzi R, Negro E, Vittadello M, Pace G. Hybrid inorganic-organic proton conducting membranes based on Nafion and 5 wt.% of M_xO_y (M = Ti, Zr, Hf, Ta and W). Electrochim Acta 2007;53:1618–27.

[36] Di Noto V, Lavina S, Negro E, Vittadello M, Conti F, Piga M, et al. Hybrid inorganic-organic proton conducting membranes based on Nafion and 5 wt% of M_xO_y (M = Ti, Zr, Hf, Ta and W). Part II: relaxation phenomena and conductivity mechanism. J Power Sources 2009;187:57–66.

[37] Vittadello M, Negro E, Lavina S, Pace G, Safari A, Di Noto V. Vibrational studies and properties of hybrid inorganic-organic proton conducting membranes based on Nafion and hafnium oxide nanoparticles. J Phys Chem B 2008;112: 16590–600.

[38] Di Noto V, Piga M, Piga L, Polizzi S, Negro E. New inorganic-organic proton conducting membranes based on Nafion® and $[(ZrO_2)\cdot(SiO_2)_{0.67}]$ nanoparticles: synthesis, vibrational studies and conductivity. J Power Sources 2008;178:561–74.

[39] Di Noto V, Piga M, Lavina S, Negro E, Yoshida K, Ito R, et al. Structure, properties and proton conductivity of Nafion/ $[(TiO_2)\cdot(WO_3)_{0.148}](\psi TiO_2)$ nanocomposite membranes. Electrochim Acta 2010;55:1431–44.

[40] Di Noto V, Negro E, Lavina S, Vittadello M. Hybrid inorganic-organic polymer electrolytes. In: Sequeira C, Santos D, editors. Polymer electrolytes - fundamentals and applications. Cambridge: Woodhead Publishing Limited; 2010. p. 219–77. vol.

[41] Thayumanasundaram S, Piga M, Lavina S, Negro E, Jeyapandian M, Ghassemzadeh L, et al. Hybrid inorganic–organic proton conducting membranes based on Nafion, SiO_2 and triethylammonium trifluoromethanesulfonate ionic liquid. Electrochim Acta 2010;55:1355–65.

[42] Di Noto V, Boaretto N, Negro E, Pace G. New inorganic–organic proton conducting membranes based on Nafion and hydrophobic fluoroalkylated silica nanoparticles. J Power Sources 2010;195:7734–42.

[43] Di Noto V, Negro E, Sanchez J-Y, Iojoiu C. Structure-relaxation interplay of a new nanostructured membrane based on tetraethylammonium trifluoromethanesulfonate ionic liquid and neutralized Nafion 117 for high-temperature fuel cells. J Am Chem Soc 2010;132:2183–95.

[44] Di Noto V, Negro E. Pt–Fe and Pt–Ni carbon nitride-based "Core-Shell" ORR electrocatalysts for polymer electrolyte membrane fuel cells. Fuel Cells 2010;10:234–44.

[45] Kocha SS. Principles of MEA preparation. In: Vielstich W, Lamm A, Gasteiger HA, editors. Handbook of fuel cells: fundamentals technology and applications, vol. 3. Chichester: John Wiley & Sons; 2003. p. 538–65.

[46] Gasteiger HA, Kocha SS, Sompalli B, Wagner FT. Activity benchmarks and requirements for Pt, Pt-alloy, and non-Pt oxygen reduction catalysts for PEMFCs. Appl Catal B 2005;56:9–35.

[47] Zawodzinski Jr TA, Neeman M, Sillerud LO, Gottesfeld S. Determination of water diffusion coefficients in perfluorosulfonate ionomeric membranes. J Phys Chem 1991; 95:6040–4.

[48] Spiegel CS. Designing and building fuel cells. New York: McGraw-Hill; 2007.

[49] Hofmann DWM, Kuleshova L, D'Aguanno B, Di Noto V, Negro E, Conti F, et al. Investigation of water structure in Nafion membranes by infrared spectroscopy and molecular dynamics simulation. J Phys Chem B 2009;113:632–9.

[50] Ochi S, Kamishima O, Mizusaki J, Kawamura J. Investigation of proton diffusion in Nafion 117 membrane by electrical conductivity and NMR. Solid State Ionics 2009;180:580–4.

[51] Perrin J-C, Lyonnard S, Volino F. Quasielastic neutron scattering study of water dynamics in hydrated Nafion membranes. J Phys Chem C 2007;111:3393–404.

[52] Di Noto V, Lavina S, Negro E, Pace G. FUEL 113-Structure and interactions in Nafion® core-shell oxoclusters hybrid proton-conducting membranes. Abstr Pap Am Chem Soc 2008;236.

[53] Di Noto V. Zeolitic inorganic-organic polymer electrolyte based on oligo(ethylene glycol) 600 K_2PdCl_4 and $K_3Co(CN)_6$. J Phys Chem B 2000;104:10116–25.